An Objective High-Resolution Hail Climatology of the Contiguous United States

John L. Cintineo[1,*]
Cooperative Institute of Meteorological Mesoscale Studies, University of Oklahoma and National Severe Storms Laboratory, Norman, Oklahoma

Travis M. Smith
Cooperative Institute of Meteorological Mesoscale Studies, University of Oklahoma and National Severe Storms Laboratory, Norman, Oklahoma

Valliappa Lakshmanan
Cooperative Institute of Meteorological Mesoscale Studies, University of Oklahoma and National Severe Storms Laboratory, Norman, Oklahoma

Harold E. Brooks
National Severe Storms Laboratory (NSSL), Norman, Oklahoma

Kiel L. Ortega
Cooperative Institute of Meteorological Mesoscale Studies, University of Oklahoma and National Severe Storms Laboratory, Norman, Oklahoma

[1] *Corresponding author address*: John L. Cintineo, CIMSS, University of Wisconsin – Madison, 1225 W. Dayton St., Madison, WI 53706.
E-mail: john.cintineo@ou.edu
* Current affiliation: Cooperative Institute of Meteorological Satellite Studies (CIMSS), Madison, WI.

Abstract

The threat of damaging hail from severe thunderstorms affects many communities and industries on a yearly basis, with annual economic losses in excess of 1 billion U.S. dollars. Past hail climatology has typically relied on National Oceanic and Atmospheric Administration's (NOAA) National Climatic Data Center's (NCDC) *Storm Data*, which has numerous reporting biases and non-meteorological artifacts. This research seeks to quantify the spatial and temporal characteristics of contiguous U.S. (CONUS) hail fall, derived from multi-radar multi-sensor (MRMS) algorithms for several years during the Next-Generation Radar (NEXRAD) era, leveraging the Multi-Year Reanalysis Of Remotely Sensed Storms (MYRORSS) dataset at NOAA's National Severe Storms Laboratory (NSSL).

The primary MRMS product used in this study is the maximum expected size of hail (MESH). The preliminary climatology includes 42 months of quality-controlled and re-processed MESH grids, which spans the warm seasons for 4 years (2007-2010), covering 98% of all *Storm Data* hail reports during that time. The dataset has 0.01^{o} latitude x 0.01^{o} longitude x 31 vertical levels spatial resolution, and 5-minute temporal resolution. Radar-based and reports-based methods of hail climatology are compared. MRMS MESH demonstrates superior coverage and resolution over *Storm Data* hail reports, and is largely unbiased. The results reveal a broad maximum of annual hail fall in the Great Plains and a diminished secondary maximum in the southeast U.S. Potential explanations for the differences in the two methods of hail climatology are also discussed.

1. Motivation

The annual damage due to hail in the United States in 1999 was an estimated 1.2 billion U.S. dollars, accounting for crop and property losses (Changnon 1999), and has likely increased since then. Due to the high economic vulnerability in the U.S., research on the nature of hail has been ongoing for decades. Hail climatology, and severe weather climatology in general, provides an important record of past events and historical trends, which have a myriad of implications including severe weather forecasting, insurance industry purposes, agriculture concerns, and climate change indicators. However, most U.S. hail climatology relies on the National Oceanic and Atmospheric Administration's (NOAA) National Climatic Data Center (NCDC) *Storm Data* severe weather reports database or other ground reports (Doswell et al. 2005, Kelly et al. 1985, Changnon and Changnon 2000), which have many documented biases and reporting artifacts (Trapp et al. 2006, Doswell et al. 2005, Witt et al. 1998b, Hales 1993, Kelly et al. 1985, Morgan and Summers 1982). Storm Data records reports from the public, with no designated reporting stations. These reports almost always neglect non-severe hail, are biased toward the low-end of severity, and are influenced heavily by population density and other non-meteorological factors (Hales 1993). Schaefer et al. (2004) point out that the dramatic increase in the number of hail reports in the last century is due to non-meteorological factors, and that the distribution of historical hail sizes in reports is quantized. Furthermore, since severe storm verification by the National Weather Service (NWS) has spatial and temporal scales comparable to associated severe weather warnings (Hales and Kelly 1985), on the order of 1000 km^2 and tens of minutes (Ortega et al.

2009), this study employs a high-resolution tool that meteorologists use to observe hail-producing storms—weather radar.

The contiguous United States (CONUS) has one of the most dense and robust networks of weather radars in the world, consisting principally of the NWS Weather Surveillance Radar – 1988 Doppler (WSR-88D) network, often termed “next generation” radar system (NEXRAD). The network of Terminal Doppler Weather Radars (TDWR) established by the Federal Aviation Administration is also an extensive CONUS radar network, which scans for hazardous weather at many American airports. NEXRAD and the TDWR network have been valuable tools for severe weather diagnosis for NWS forecasters since their inception (Mitchell and Elmore 1998). Among these hazards are hail, severe winds, flash-flooding, and tornadoes. There have been numerous automated attempts to identify and nowcast (short-term forecast, usually in a warning-issuing context) hail from severe thunderstorms using radar data (e.g. Waldvogel 1979, Mather et al. 1976, Amburn and Wolf 1997, Ortega et al. 2005, Witt et al. 1998a, Marzban and Witt 2001). Since the establishment of NEXRAD in 1994, Level-II radar moment data has been stored at NOAA NCDC, which consists of approximately 15 years of radar volume scans at the writing of this paper.

This research leverages the Multi-Year Reanalysis Of Remotely Sensed Storms (MYRORSS) dataset, developed at NOAA’s National Severe Storms Laboratory (NSSL) (Cintineo et al. 2011). This dataset uses Level-II radar information and 20-km Rapid Update Cycle (RUC) analysis fields to create multi-radar multi-sensor (MRMS) severe weather algorithms, including hail diagnosis products, such as the maximum expected size of hail (MESH). The purpose of the study is two-fold: 1) To create a CONUS hail climatology derived from NEXRAD data, which is objective, has high spatiotemporal resolution, and is quantitatively accurate and 2) To demonstrate the utility of this high-resolution dataset for future severe weather analysis.

This paper is organized as follows: section 2 describes the means of creating the MYRORSS dataset and the method of producing the hail climatology; section 3 demonstrates the results of this work; section 4 explains differences between radar-based and reports-based hail climatology; and section 5 summarizes the outcomes of this research.

2. Methodology

a. Creating the MYRORSS dataset

The main challenge of creating the MYRORSS database is tackling the shear volume of data to be analyzed. Every volume scan for every radar (134 in the CONUS) was reprocessed for the 42 months investigated in this climatology, which exceeded 30 million volume scans. The months processed are: January through December in 2010 and 2009, March through December in 2008, and March through October in 2007. In order to process this large amount of CONUS WSR-88D data, many different machines at NSSL were employed with their computational power maximized by utilizing idle CPU cycles. The Warning Decision Support System – Integrated Information (WDSS-II) is the tool used to quality control (QC) and process the data (Lakshmanan et al. 2007b).

The standard configuration set in place for processing radar data includes seven server machines (12-48 GB of RAM), twelve machines used for seasonal projects (12-16 GB of RAM), and eight other desktop machines (8 GB of RAM). The seasonal and other desktop machines are “farm” machines, which handle the single-radar processing. Raw Level-II data was downloaded from NCDC for all CONUS radars in monthly increments. The main server, or “master” server, controls the flow of processing and delegates jobs to the 20 farm machines. Each “job” represents processing an individual CONUS radar for one hour, if it contains super-resolution data (Torres and Curtis, 2007), or for an eight-hour block, if it is of legacy resolution. The first step of single-radar processing is to QC the reflectivity using a WDSS-II algorithm (Lakshmanan et al. 2007a), which employs a neural network to censor artifacts such as radar clutter, anomalous propagation, radials of electronic interference, and biological echoes (Lakshmanan et al. 2010), while maintaining valid precipitation echoes. The QC step also includes dealiasing Doppler velocity data, which is performed by ingesting near storm environment (NSE) atmospheric soundings from the radar sites. The WDSS-II NSE algorithm processes gridded 20-km RUC analysis fields to produce many environmental parameters that are ingested by other algorithms, namely hail detection and diagnosis applications (Lakshmanan et al. 2007b). Among these products is an hourly sounding over each radar site. The sounding is used to dealias radial velocity for an entire hour for that radar. Dealiasing is not important for the MESH algorithm, but is for velocity-derived products, such as merged azimuthal shear (AzShear) (Smith and Elmore, 2004).

The AzShear is sent back to the master server, and archived on a 54 TB storage disk. The single-radar QC reflectivity is sent to one of four servers that are used for blending, or “merging” the data into a three-dimensional (3D) cube of reflectivity, termed MergedReflectivityQC. This product has 0.01^{o} latitude x 0.01^{o} longitude (about 1 x 1 km in the midlatitudes) x 31 vertical levels spatial resolution, and 5-minute temporal resolution. The single-radar processing and reflectivity blending occur in parallel among 20 farm machines and 4 servers. The blending weights reflectivity using an inverse-squared distance method, which is one of several weighting options. Lakshmanan et al. (2006) fully describes the WDSS-II data-merging algorithm. Essentially, the algorithm creates a best estimate of a Level-II radar moment from all nearby sensing radars by accounting for varying radar beam geometry with range, vertical gaps between radar scans, lack of a time synchronization between radars, storm motion, varying beam resolutions between different types of radars, beam blockage due to terrain, and differing radar calibration. MergedReflectivityQC is blended in daily increments.

Post-processing algorithms use the 20-km RUC analysis fields and the 3D cubes of MergedReflectivityQC to create an assortment of CONUS-wide two-dimensional (2D) grids of MRMS products (e.g. MESH, reflectivity at -20^{o}C), with horizontal and temporal resolution identical to the MergedReflectivityQC. Low-level and mid-level AzShear fields are also merged to create CONUS 2D grids. All of the MRMS and velocity-derived products found in TABLE 1 are archived in the MYRORSS database. The goal is to make this database publicly available through NCDC within three years.

b. Creating a radar-based hail climatology

1) THE USEFULNESS OF MESH

MESH was originally developed as part of the enhanced hail detection algorithm (HDA) at NSSL by Witt et al. (1998a) and was derived empirically from the Severe Hail Index (SHI).

$$MESH=2.54(SHI)^{0.5}$$

The “size” in MESH refers to the maximum diameter (in mm) of a hailstone. SHI is a thermally weighted vertical integration of reflectivity from the melting level to the top of the storm, neglecting any reflectivity less than 40-dBZ, thereby attempting to capture only the ice content of a storm (Witt et al. 1998a). MESH was originally tuned to be a cell-based algorithm (i.e. one MESH value per storm identification per volume scan), but has been converted into a grid-based algorithm with the advent of high-resolution MRMS products. MESH was calibrated using 147 hail observations from 9 storm days based on data from radar sites in Oklahoma and Florida. It was developed such that 75% of the hail observations would be less than the corresponding predictions (Witt et al. 1998a), since using the largest observation could have introduced noise into the calibration.

Using reflectivity from multiple nearby radars offer more accurate depictions of storms by over-sampling, especially for storms at far ranges from one radar, storms in the cone of silence of a radar, and where the terrain is blocking storm surveillance (Stumpf et al. 2004). Stumpf et al. (2004) explain how the use of MRMS algorithms improve SHI, probability of severe hail (POSH), MESH, and composite reflectivity estimates. Ortega et al. (2005) note that both multi-radar cell-based and Cartesian grid-based techniques substantially outperform the single-radar MESH in their preliminary comparisons. Ortega et al. (2006) compared verification scores of MESH against *Storm Data* for three different methods: single-radar, cell-based MESH; multi-radar, gridded MESH; and multi-radar, cell-based MESH. Variations on these methods were also tested, such as time and space correction and storm tilt correction. It was shown again that the multi-radar techniques performed much better than the single-radar MESH, and that time/space corrections (based on a storm segmentation and motion estimation method from Lakshmanan et al. 2003 and Lakshmanan et al. 2009) and storm tilt corrections helped decrease the root mean squared error for both gridded and cell-based techniques appreciably, though gridded techniques overall resulted in lower error than cell-based.

It is now clear that 2D gridded fields of hail size based on integration of a 3D reflectivity field have many advantages over the single-radar enhanced HDA. However, hail detection and hail size estimation is imperfect. Ortega et al. (2009) describe the Severe Hazard and Analysis Verification Experiment (SHAVE) at NSSL, which collects high-resolution severe hail reports, as well as non-severe and no-hail reports, for storms across the U.S. during the warm season (April – August), which are used to evaluate MRMS algorithms. Wilson et al. (2009) use SHAVE reports to evaluate MESH and other MRMS products. They found that while MESH outperforms the vertically integrated liquid (VIL) predictor, it was not skillful for one-to-one hail size prediction. MESH was found to have an overforecasting bias (partly by design), which led to a relatively high probability of false detection, and low Heidke Skill Score (HSS) (Wilks 2006). It is emphasized that our study uses the multi-radar MESH product to detect the presence of any hail and severe hail. Therefore, it is used as a verification tool and not as a predictor of exact hail size.

2) OPTIMAL MESH THRESHOLDS

The next step is to determine optimal sizes of MESH that correspond well with thresholds of actual hail. The two thresholds of interest are 1) any hail and 2) severe hail. Severe hail is defined as hail with 19 mm diameter or greater, in order to make this analysis more comparable with reports-based severe hail climatology during the NEXRAD era (e.g., Doswell et al. 2005).

To find these optimal thresholds, high spatiotemporal resolution hail reports from SHAVE were interrogated. The SHAVE data consisted of 144 storms from throughout the CONUS on 86 days over 2006-2009. The multi-radar MESH threshold was varied from 1 to 60 mm, in order to find the threshold that maximizes the HSS about all of the reports. MESH swaths were overlaid with SHAVE reports, illustrated in FIG. 1 (from Wilson et al. 2009). In a neighborhood of 2 km around each report, the median, maximum, and point-match MESH were obtained (2 km was chosen since that is the approximate horizontal resolution of SHAVE reports). For a given hail size threshold, a "hit" was made when both the MESH and SHAVE report were greater than the threshold. A "miss" was made when the MESH was below the given threshold, but the SHAVE report was above the threshold. A "false alarm" was when the SHAVE report was below the threshold, but the MESH was above the threshold, and a "correct null" was when both measures were below the threshold. Aggregating these statistics for all of the reports, the HSS was computed for each MESH size. For the "any hail" threshold, the highest HSS was 0.39 for the median MESH statistic, at a size of 21 mm. For "severe hail" SHAVE reports (19 mm), the highest HSS was 0.40 for the median MESH, at a size of 29 mm. These optimal skill thresholds are illustrated in FIG. 2.

The skill scores were broken down by region to investigate the effect different geographical areas may have on MESH. East of the Rocky Mountains, the U.S. was divided into four quadrants: the northern Plains (NW—3951 SHAVE reports), southern Plains (SW—2421 reports), the Midwest, Mid-Atlantic and New England (NE—1141 reports), and the southeast U.S. (SE—1514 reports). The region west of the Rockies was not included do to an insufficient number of reports (65). The HSS for each region is shown in FIG. 2 for MESH of 21 mm, 29 mm, and the maximum HSS obtained (for the severe hail threshold). The NW, SW, and SE quadrants all show comparable skill (HSS ≥ 0.35), whereas the NE quadrant demonstrates somewhat lower skill (0.25 – 0.28). Given that the peak skill in the SE was achieved at 24 mm, and in the SW was achieved at 34 mm, it is possible that our single threshold of severe hail (29 mm) may be slightly overestimating hail fall in the SW, and slightly underestimating in the SE. The diminished skill in the NE may be a result of the lower number of reports, but does merit further analysis. Since the maximum HSS for each region was achieved near 29 mm, and each region had comparable skill (except perhaps the NE), a single most-skillful threshold to delineate severe hail is justified, and used for simplicity.

It is the opinion of the authors that the very high resolution of the reports in SHAVE illustrates the high variability of hail fall within a storm. Hail may often be driven by the updraft out of the storm and fall to the surface at locations away from the storm, with different MESH values from where the hail was produced. This may result in the “double penalty” of getting a false alarm and a miss. For these reasons, the HSS of MESH cannot adequately be compared to prior studies (e.g., Kessinger et al. 1995, Witt et al. 1998a). However, such HSS for high-resolution MESH deem the algorithm skillful at detecting hail and therefore make it useful as a verification tool for hail fall.

The MESH thresholds of 21 mm and 29 mm are used throughout the remainder of this paper as the “any hail” and “severe hail” criteria, respectively. The threshold for significant severe hail (defined as 50.8 mm diameter by convention) was also sought. However, MESH produced little skill in discerning this threshold (HSS $\leq$ 0.10 for all MESH values, likely due to the “double penalty” opined above) and therefore an analysis for significant hail detection with MESH is not provided. SHAVE reports from more cold-season storms and NE storms should be gathered in the future to further evaluate MESH, to make the validation even more robust.

3) MESH-DERIVED GRIDS

The MESH grids with 5-minute temporal resolution were accumulated for contiguous 24-hour periods, taking the maximum MESH value at every pixel in the CONUS, creating daily MESH grids. FIG. 3 shows an example of a daily MESH grid, from the Midwest U.S. Note that entire swaths of hail for storms can be depicted. Despite the QC process, some reflectivity (and therefore MESH) errors still exist (e.g. radial fragments in south-central Nebraska in FIG. 3), however, reflectivity errors below 0^{o} C won't affect MESH. By creating daily MESH grids, it is possible to isolate MESH artifacts in an efficient manner and remove them. Daily MESH grids were hand-examined (searching for anomalous propagation or electronic interference spikes), and errors were removed manually by cropping the region out. If areas of real MESH were in close proximity to artificial MESH, the artificial MESH was removed in a 5-minute grid instead of the daily grid. Once the bad MESH regions are removed, new QC daily MESH grids were created.

With the daily MESH grids, several maps of hail threat were explored. A yearly accumulation of MESH is examined, demonstrating the maximum threat of hail for a year or collection of years for any single point. Next, "count maps" were created by accumulating counts of MESH exceeding a threshold (21 mm or 29 mm) in the daily MESH grids. Thus, this is equivalent to creating a "hail days" map – the number of days in a year (or per year) that any grid point experienced hail or severe hail. Monthly hail maps are also created, to illustrate the seasonal cycle of hail in the U.S.

c. Challenges using NEXRAD data

There are several challenges in using NEXRAD data in an historical sense, each with some inherent error, which will be discussed briefly. Some of these are accounted for and mitigated, while some are more difficult to address.

Terrain blockage of the radar beam is largely absent in the eastern two-thirds of the U.S. (see section 4 and FIG. 12). Locales in mountainous regions in the west and some parts of the Appalachians in the east may be prone to this bias. However, the multiple radar coverage largely mitigates this bias in the eastern U.S. In regions of single-radar coverage (e.g. Big Bend of southwest Texas), beam widening becomes a problem. The resolution volume of the radar is very large at far ranges. When a precipitation echo is present in this volume, the radar will fill the entire resolution volume with the reflectivity value of that precipitation, even if it is only present in a small fraction of the volume. Thus, strong reflectivity may be spatially overestimated, potentially creating a bias of too much hail fall in MESH. Again, when there is multiple radar coverage, the distance weighting for each radar diminishes this bias and creates better reflectivity estimates.

Some non-meteorological echoes already mentioned that can bias this climatology include radial spikes from electronic interference, anomalous propagation, and biological “blooms” around a radar (from birds, bats, or insects). The WDSS-II QC algorithm does an excellent job eliminating most of these echoes, but even a highly efficient QC algorithm will miss artifacts in 30 million volume scans, due to the diversity of radar echoes. To further eliminate errors, subjective QC was carried out on the MESH grids manually (as described above). These steps help mitigate errors, but do not eliminate all of the artifacts.

One other challenge to contend with is differing radar calibration. The Radar Operations Center (ROC) actively monitors NEXRAD data in real-time. When adjacent radar estimates of reflectivity differ by a lot, they are recalibrated. By using historical reflectivity, this is a problem that cannot be adequately addressed since the “true” reflectivity is unknown. However, any bias should be small in nature, considering the length of the study. Furthermore, radar calibration differences are mitigated somewhat using estimates from neighboring radars in the merging process.

3. Results

This section will describe annual hail maps for 2007-2010, as well as monthly composites for the four years. The climatology is relatively short in terms of number of years, but the authors aim to complete a NEXRAD era CONUS hail climatology in the next three years.

Daily MESH grids from all 12 months of 2009 and 2010 were created for analysis. The months of March through December were processed in 2008, and March through October was processed for 2007. These 42 months span 98% of the *Storm Data* hail reports during the full four years. With the daily MESH grids, we first may investigate the accumulation of MESH over the four years, taking the maximum MESH at every grid point (FIG. 4). This gives an idea of the maximum hail threat each grid point experienced in 2007-2010. A main broad swath of high MESH values in the Great Plains is very evident. This triangular region of hail fall extends from southwest Texas, northeastward to northwest Missouri, then northwestward into western South Dakota, and finally down the front range of the Rocky Mountains, into eastern New Mexico and west Texas. Maximum hail size diminishes eastward from this corridor, into Minnesota, Iowa, Illinois, Missouri, Arkansas, eastern Oklahoma, and eastern Texas. Several other regions of enhanced MESH swaths are along the East Coast, from eastern Pennsylvania through Florida, but most prevalent in South Carolina and Georgia.

Count maps were created for each of the four years and averaged to obtain hail days and severe hail days per year. These annual hail day maps were smoothed using three successions of 90% and 25% filters, in a 0.11^{o} x 0.11^{o} neighborhood. The percentile smoothing was performed with a “storm-scale” radius of approximately 10 km, in order to reduce noise within MESH swaths, yet still maintaining the swaths themselves. A Gaussian filter was then applied, with a 0.51^{o} x 0.51^{o} kernel and a smoothing radius equal to three standard deviations, since the function is nearly zero at that radius (i.e. values at the edge of the window have very little weight). This smoothing fills in MESH-free gaps between individual hail swaths that are present merely as a result of high-variability in the four years of this study. FIG. 5 and FIG. 6 demonstrate the annual number of hail days and severe hail days, respectively, for 2007-2010. From FIG. 6, we see the triangular corridor in the Plains of more frequent severe hail (0.5 to 1 day), tailing off to roughly 0.25 days in neighboring states. The southeast U.S. has only a few pockets of 0.25 severe hail days, in Virginia, South Carolina, and Georgia. The relatively low frequency of severe hail days is a product of the very high resolution of the dataset, as well as the high variability of hail-producing storms in the four years. FIG. 5 is spatially very similar to FIG. 6, but with higher frequencies throughout.

Composite monthly severe hail maps were created using the same count and smoothing method as the four-year annual hail maps. January through June and July through December are shown in FIG. 7 and FIG. 8, respectively. All four years contribute to the hail day averages of March through October, while November and December have three contributing years (2008-2010) and January and February have two (2009 and 2010). Very little severe hail is observed in January and February, while in March and April an enhanced hail threat begins to build in the southern U.S. By May, the southern Plains hail threat is prevalent, with regions of 0.1 to 0.4 hail days per year. June clearly is the leading month for severe hail, and the largest contributor to the triangular maximum of hail days. Southeast U.S. hail fall also reaches its maximum. In July and August, the hail threat drifts northward to the northern and central Plains. By September, hail threat has greatly diminished, with the strongest intensity of hail days in the Plains (0.1 days). October reduces the hail threat even more, as the main hail day zone is now located in the southern U.S. and Gulf Coast. November and December are devoid of severe hail.

4. Comparison with Past Climatology

Hail climatology is an extensive topic that has been investigated in depth by a number of researchers. Some research has focused on hail at a regional scale (Cheresnick et al. 2004, Nelson and Young 1979, Changnon et al. 1967), while other researchers employed storm reports on a national scale (Doswell et al. 2005, Kelly et al. 1985, Changnon and Changnon 2000), while still others employed radar algorithms to diagnose hail (Cheresnick et al. 2004, Saltikoff et al. 2010). Brooks and Lee (2003) used the National Centers for Environmental Prediction (NCEP)/National Center for Atmospheric Research (NCAR) 40-year reanalysis data set (Kalnay et al. 1996) to examine the history of hailstorm-conducive environments in the United States and worldwide. This was done in part to mitigate reporting biases and inconsistencies through time and among regions of the globe. Cheresnick et al. (2004) investigated hail swaths over a three-year period derived from radar-based algorithms in the state of Oklahoma. Saltikoff et al. (2010) investigated hailstorms for five summers in Finland using radar data, while corroborating their findings with the newspaper reports from Tuovinen et al. (2009). Cecil and Blankenship (2011) use passive microwave satellite data from the Advanced Microwave Scanning Radiometer for Earth Observing System (EOS) (AMSR-E) and the Tropical Rainfall Measuring Mission (TRMM) Microwave Imager (TMI) to estimate worldwide hail frequency. However, AMSR-E spatial resolution is quite coarse (14 x 8 km at the 36.5 GHz channel) and the temporal coverage is incomplete, as AMSR-E is aboard the National Aeronautic and Space Administration’s (NASA) Aqua satellite, which is in a sun-synchronous orbit. Furthermore, TMI is limited spatially to the tropics and parts of the subtropics (+/- 38^{o} latitude), and has limited temporal resolution.

What makes this study unique is that it uses high-resolution MRMS MESH to investigate the character of hail fall over the CONUS. Since reports-based hail climatology is the most familiar source for hail statistics in the U.S., we seek to compare hail frequency maps from the radar-based method of this paper to reports-based method of Doswell et al. (2005).

a. Event Day Methodology

Doswell et al. (2005) and Brooks et al. (2003) employ a strategy termed "event day methodology" in order to mitigate reporting biases in *Storm Data* and to isolate the strongest signals for hail fall in the U.S. This paper uses their method to appropriately compare the radar-based and reports-based approaches.

Firstly, a CONUS-wide grid of dimensions I x J with grid-box resolution of 0.8^{o} x 0.8^{o} is initialized with zeroes for the nth day of the year. A grid box is turned "on" (m = 1 for a single year; m = 0.25 for the four year period) if one or more events occurs on that day in the spatial bounds of the (x, y)-grid box, thus making each daily event grid binary. An event for the reports-based method is straightforward—a severe hail report (diameter ≥ 19 mm) in the grid box. An event for the radar-based method was chosen using heuristics. The threshold for an event was deemed to be at least five pixels (at 0.01^{o} horizontal resolution) of MESH ≥ 29 mm. The criterion of five pixels helps reduce noise and the criterion of MESH ≥ 29 mm ensures severe hail is identified. Once daily event grids are created for each day, a temporal Gaussian filter is applied,

$$f_n = \sum_{k=1}^{366} \frac{m}{\sqrt{2\pi\sigma_t}} \exp\left[-\frac{1}{2}\left(\frac{n-k}{\sigma_t}\right)^2 \right]$$

where σ_t = 15 days (the temporal smoothing parameter), k is the index for day of the year, and f_n is the smoothed value for the nth day. A spatial Gaussian filter is subsequently applied,

$$p_{x,y,n} = \sum_{j=1}^{J}\sum_{i=1}^{I} \frac{f_n}{2\pi{\sigma_x}^2} \exp\left[-\frac{1}{2}\left(\frac{d_{i,j}}{\sigma_x}\right)^2 \right]$$

where $p_{x,y,n}$ is the mean expected number of event days for the certain criterion per year, σ_x = 1.5 grid boxes (the spatial smoothing parameter), or 1.2^{o}, and $d_{i,j}$ is the Euclidean distance between analysis location (x, y) and data location (i, j), in grid-point space. See Doswell et al. (2005) or Brooks et al. (2003) for a complete description of the event day methodology.

b. Annual severe hail days

Using the event day methodology, and the criteria of at least five pixels of MESH ≥ 29 mm, the annual number of severe hail days was computed for the radar-based method of this paper using 42 months over 2007-2010, shown in Fig. 9 (nearest-neighbor linear interpolation was applied to the 0.8^{o} x 0.8^{o} grids in Figs. 9 – 11). The triangular corridor of hail in the Great Plains remains the strongest signal by far, at 11-12 days. There are appendages of secondary maxima in northeast Texas/southwest Arkansas (7 days), southern Arizona (4-5 days), and eastern Montana (4-5 days). Along the east coast, from Maryland into Florida, there is another maximum of 5-6 days.

Using *Storm Data* hail reports of 19 mm diameter or greater, the annual number of severe hail days was also computed, shown in FIG. 10. It should be noted that both radar-based and reports-based hail day maps are over the same time period. The reports-based severe hail map shows an oval-shaped maximum of hail days in the Plains (7-10 days), covering Nebraska, northeast Colorado, Kansas, and Oklahoma. There is still an appendage of hail days extending into eastern Montana (2-4 days), but a dearth of hail days in west Texas, eastern New Mexico, and Arizona. There is also a significant maximum over western North and South Carolinas (7-9 days), as well as smaller pockets of hail days in Ohio (4 days), Mississippi (6 days), and southern New England and New York (5 days).

The radar-based hail days (FIG. 9) subtracted from the reports-based hail days (FIG. 10) produces a severe hail day difference map for 2007-2010 (FIG. 11), illustrating hail day deficits (less than zero) and hail day surpluses (greater than zero). Strong hail day deficits are evident in parts of the Plains, including southwest Texas (-8 to -9 days), northeast New Mexico (-7 to -8 days), and northwest Nebraska and southwest South Dakota (-5 days). There are also hail day deficits in Florida (-2 days) and Louisiana and southeast Texas (-2 to -3 days). Hail day surpluses are manifest in parts of the eastern United States, namely western Virginia through northern Georgia (+3 to +5 days), Ohio, southern New York and New England (+2 days), and Mississippi (+1 to +2 days).

The largest hail day deficits are readily explained by few hail reports on account of very low population density (e.g. southwest Texas, northeast New Mexico, northwest Nebraska). Davis and LaDue (2004) found a strong correlation between population density and reports density, which is consistent with the findings of Wyatt and Witt

(1997) and Hales (1993). However, southwest Texas has limited low-level radar coverage, which contributes to an elevated beam height (over 10,000 ft) and becomes subject to the beam-spreading problem. See FIG. 12 for a map of NEXRAD coverage below 10,000 ft (ROC 2011). Here, overestimates of hail are possible, since the resolution volume at this range is relatively large (several cubic km) and may be entirely assigned with a high reflectivity, even if it is only partially filled with high reflectivity in actuality. Furthermore, if the melting level is below 10,000 ft where reflectivity is present, the MESH algorithm will create an underestimate. The large deficit of hail days in southwest Texas is most likely due to a combination of sparse population and the effects of beam-spreading/single-radar coverage in this region.

Smaller hail day deficits exist in regions of larger population centers, such as Louisiana, Florida, and southeast Texas. These parts of the country have a climate regime more tropical in nature, often marked by warmer temperatures and higher relative humidity in the boundary layer and perhaps mid-levels of the atmosphere. Despite the fact that the calibration of MESH used some storms from central Florida (Witt et al. 1998a), the unique boundary layer atmosphere of the Gulf Coast may account for the hail day deficits. In a warmer, more humid environment, hailstones tend to melt more efficiently (Straka 2009), as evaporative cooling from melt water on the hailstones becomes less effective at cooling the surface of the hailstone, due to the ambient high relative humidity. It is also plausible that hailstones aloft are not that large to begin with, as the steep mid-level lapse rates exhibited in the central Plains (due to the region's proximity to the Rocky Mountains) become much less pronounced toward the southeast U.S. and Gulf Coast, contributing to less buoyancy in the middle troposphere, creating smaller hailstones. Melting would be intensified by higher 0^{o} C isotherms (e.g., Xie et al. 2010). Therefore, a collection of small severe-sized hailstones aloft (detected by radar) can melt efficiently in the boundary layer of such a climate, which could make the radar-based estimates artificially high. Xie et al. (2010) demonstrate that for a melting level height of 4.5 km, a 25.4 mm diameter hailstone will melt to about 20.3 mm. This difference in size is barely resolvable in *Storm Data* reports, given their quantized nature (Schaefer et al. 2004). Thus, melting is indeed important for small hailstones (and perhaps marginally severe hail), but is negligible for larger severe-sized hailstones, given the reporting accuracy of *Storm Data.*

The hail surplus days may be occurring for several reasons. One explanation may be radar beam blockage (in parts of the Appalachian Mountains) and other radar geometry problems. However, based on FIG. 12, the effects should be minimal, and include small regions in southwest North Carolina, northern Virginia, southeast Pennsylvania, and eastern Vermont. These regions would have minor impacts on this climatology, and most likely underestimate hail fall only when storms are shallow or behind mountains. Another possible explanation is NWS Weather Forecast Office (WFO) bias and heterogeneity in verification of thunderstorms. NWS WFOs only require one report of any severe weather (hail, wind, or tornado) to verify a warning (NWS 2011). Offices that issue numerous warnings on marginally severe storms may make earnest efforts to verify their warnings, even if the vast majority of the hail fall in the storm is well below the severe criterion. Therefore, marginally severe thunderstorms may go undetected by the MESH severe hail threshold in this paper, while a WFO makes strong attempts at verification. Other explanations of hail day surplus include inaccurate environment information from the 20-km RUC analysis (such as errors in the height of the 0^{o} C isotherm), and inadequate calibration of the original MESH with SHI for certain regions (southeast, northeast U.S.). These differences should be explored in detail when a longer climatology is available.

5. Summary

This research has presented an objective CONUS hail climatology with very high spatiotemporal resolution over four years. The resolution and coverage of this climatology far exceeds that of reports-based methods, and reveals some features of hail fall not found in reports-based climatology. A triangular corridor of severe hail is evident from southwest Texas, extending east to Missouri, and north to South Dakota. There is excellent multi-radar coverage in this region, except in the Big Bend region of southwest Texas. The monthly hail maps shows an annual cycle of enhanced hail frequency in the Great Plains during the months of March through September. In March through May, the southern Plains and parts of the southeast U.S. exhibit higher hail frequency, whereas the period of July through September shows larger hail frequency in the central and northern Plains. June is the most active month for hail fall, contributing mainly to the triangular corridor of hail in the Plains.

The reports-based approach shows an oval maximum of hail in the central Plains, with smaller hail frequencies than the radar-based approach, especially in west Texas, eastern New Mexico, and northwest Nebraska. Secondly, reporting-bias in the southeast U.S. (and possibly other regions) may be contributing to a more significant secondary maximum of hail fall than what is supported by radar observations. Another possible explanation for the disparity in the southeast U.S. is that MESH may not be as skillful in that region, perhaps due to more marginally severe hail events.

A complete high resolution CONUS hail climatology during the NEXRAD era is being created at NSSL using NCDC Level-II data. With the advent of the dualpolarization upgrade to the WSR-88D network and the development of polarimetric MRMS algorithms, the improvement of hail detection and hail size discrimination is promising. This capability should only advance high-resolution hail climatology over the United States.

Acknowledgments.

The authors would like to acknowledge Mike Richman for productive conversations to improve this research, as well as two anonymous reviewers for their thoughtful feedback, which greatly enhanced this manuscript. Funding was provided by NOAA High Performance Computing and Communications Office, NOAA Office of Oceanic and Atmospheric Research under NOAA-University of Oklahoma Cooperative Agreement #NA17RJ1227, and the U.S. Department of Commerce.

References

Amburn, S. A., and P. L. Wolf, 1997: VIL Density as a hail indicator. *Wea. Forecasting*, **12**, 473-478.

Brooks, H. E., 2009: Proximity soundings for severe convection for Europe and the United States from reanalysis data. *Atm. Research*, **93**, 546-553.

Brooks, H. E., C. A. Doswell III, and M. P. Kay, 2003: Climatological estimates of local daily tornado probability for the United States. *Wea. Forecasting*, **18**, 626-640.

Brooks, H. E., J. Lee, 2003: The spatial distribution of severe thunderstorm and tornado environments from global reanalysis data. *J. Atmos. Res.*, **67-68**, 73-94.

Cecil, D. J., and C. B. Blankenship, 2011: Towards a Global Climatology of Severe Hail Storms as Estimated by Satellite Passive Microwave Imagers. *J. Climate*, [in press].

Changnon, S. A., and D. Changnon, 2000: Long-term fluctuations in hail incidences in the United States. *J. Clim.*, **13**, 658-664.

Changnon, S. A., 1999: Data and approaches for determining hail risk in the contiguous UnitedStates. *J. Appl. Meteor.*, **38(12)**, 1730-1739.

Changnon, S. A., P. Schickedanz, and H. Danford, 1967: Hail patterns in Illinois and South Dakota. Preprints, *5th Conf. on Severe Local Storms*, St. Louis, MO, Amer. Meteor. Soc., 325-355.

Cheresnick, D. R., J. B. Basara, and E. D. Mitchell, 2004: An analysis of severe hail swaths in the Southern Plains of the United States. *22nd Conf. on Severe Local Storms*, Hyannis, MA, Amer. Meteor. Soc., CD-ROM, P1.34.

Cintineo, J. L., T. M. Smith, V. Lakshmanan, and S. Ansari, 2011: An automated system for processing the Multi-Year Reanalysis Of Remotely Sensed Storms (MYRORSS). *27th Conf. on Interactive Information Processing Systems*, Seattle, WA, J9.3.

Davis, S. M., and J. LaDue, 2004: Nonmeteorological factors in warning verification. *22nd Conf. on Severe Local Storms*, Hyannis, MA, Amer. Meteor. Soc., P2.7

Doswell III, C. A., H. E. Brooks, and M. P. Kay, 2005: Climatological Estimates of Daily Local Nontornadic Severe Thunderstorm Probability for the United States. *Wea. Forecasting*, **20**, 577-595.

Hales, John E. Jr., 1993: Biases in the Severe Thunderstorm Data Base: Ramifications and Solutions. *Preprints, 13th Conf. on Weather Forecasting and Analysis,* Vienna, VA, Amer. Meteor. Soc., 504-507.

Hales, J. E., Jr., and D. L. Kelly, 1985: The relationship between the collection of severe thunderstorm reports and warning verification. Preprints, *14th Conf. on Severe Local Storms*, Indianapolis, IN, Amer. Meteor. Soc., 13–16.

Kalnay, E., M. Kanamitsu, R. Kistler, W. Collins, D. Deaven, L. Gandin, M. Iredell, S. Saha, G. White, J. Woollen, Y. Zhu, A. Leetmaa, B. Reynolds, M. Chelliah, W. Ebisuzaki, W. Higgins, J. Janowiak, K. C. Mo, C. Ropelewski, J. Wang, R. Jenne, and D. Joseph, 1996: The NCEP/NCAR 40-year reanalysis project. *Bull. Amer. Meteo. Soc.*, **77**, 437-472.

Kelly, D. L., J. T. Schaefer, and C. A. Doswell III, 1985: Climatology of Nontornadic Severe Thunderstorm Events in the United States. *Mon. Wea. Rev.*, **113**, 1997-2014.

Kessinger, C. J., S. Ellis, and J. Van Andel, 2003: The radar echo classifier: A fuzzy logic algorithm for the WSR-88D. *3rd Conf. on Artificial Applications to the Environmental Sciences*, Amer. Meteor. Soc., Long Beach, CA.

Lakshmanan, V., J. Zhang, and K. Howard, 2010: A technique to censor biological echoes in radar reflectivity data," *J. Applied Meteorology*, **49**, 435-462.

Lakshmanan, V., K. D. Hondl, and R. Rabin, 2009: An efficient, general-purpose technique for identifying storm cells in geospatial images. *J. Atmos. Ocean. Tech*., **26**, 523-37.

Lakshmanan, V., A. Fritz, T. M. Smith, K. Hondl, and G. Stumpf, 2007a: An automated technique to quality control radar reflectivity data. *J. Appl. Meteor. Climatol.*, **46,** 288-305.

Lakshmanan, V., T. M. Smith, G. J. Stumpf, and K. Hondl, 2007b: The warning decision support system - integrated information. *Wea. Forecasting*, **22**, 596-612.

Lakshmanan, V., T. M. Smith, K. Hondl, G. J. Stumpf, and A. Witt, 2006: A real-time, three dimensional, rapidly updating, heterogeneous radar merger technique for reflectivity, velocity and derived products. *Wea. Forecasting*, **21**, 802-823.

Lakshmanan, V., R. Rabin, and V. DeBrunner, 2003: Multiscale storm identification and forecast. *J. Atmos. Res.*, **67**, 367-380.

Marzban, C., and A. Witt, 2001: A Bayesian neural network for severe-hail size prediction. *Wea. Forecasting,* **16**, 600-610.

Mather, G. K., D. Treddenick, and R. Parsons, 1976: An observed relationship between the height of the 45-dB*Z* contours in storm profiles and surface hail reports. *J. Appl. Meteor.*,**15,** 1336–1340.

Mitchell, E. D., and K. L. Elmore, 1998: A Technique for identifying regions of high shear associated with mesocyclones and tornadic vortex signatures. Preprints, *14th Conf. on Interactive Information Processing Systems*, Phoenix, AZ, Amer. Meteor. Soc., CD-ROM, 7.24a

Morgan, G. M., Jr., and P. W. Summers, 1982: Hailfall and hailstorm characteristics. *Thunderstorms: A Social, Scientific and Technological Documentary,* Vol. 2, *Thunderstorm Morphology and Dynamics,* E. Kessler, Ed., U.S. Government Printing Office, 363-408.

Nelson, S. P., and S. K. Young, 1979: Characteristics of Oklahoma hailfalls and hailstorms. *J. Appl. Met.*, **18**, 339-347.

NWS, cited 2011: WFO severe weather products specification. National Weather Service Instruction 10-511. [Available at http://www.weather.gov/directives/].

Ortega, K. L., T. M. Smith, K. L. Manross, K. A. Scharfenberg, A. Witt, A. G. Kolodziej, and J. J. Gourley, 2009: The Severe Hazards Analysis and Verification Experiment. *Bull. Amer. Meteor. Soc.*, 90, 1519–1530.

Ortega, K. L., T. M. Smith, G. J. Stumpf, J. Hocker, and L. Lopez, 2005: A comparison of multi-sensor hail diagnosis techniques. Preprints, *21st Conf. on Interactive Information Processing Systems,* San Diego, CA, Amer. Meteor. Soc. CD-ROM, P1.11.

Ortega, K. L., T. M. Smith, and G. J. Stumpf, 2006: Verification of multi-sensor, multi-radar hail diagnosis techniques. Preprints, *Symposium on the Challenges of Severe Convective Storms*, Atlanta, GA, Amer. Meteor. Soc. CD-ROM. P1.1

Radar Operations Center (ROC), cited 2011: NEXRAD Coverage Below 10,000 Feet AGL [Available online at http://www.roc.noaa.gov/WSR88D/Maps.aspx].

Smith, T. M. and K. L. Elmore, 2004: The use of radial velocity derivatives to diagnose rotation and divergence. Preprints, *11th Conf. on Aviation, Range, and Aerospace*, Hyannis, MA, Amer. Meteor. Soc., CD-ROM, P5.6.

Saltikoff, E., J. Tuovinen, J. Kotro, T. Kuitunen, and H. Hohti, 2010: A climatological comparison of radar and ground observations of hail in Finland. *J. Appl. Meteor. Climatol.*, **49**, 101-114.

Schaefer, J. T., J. J. Levit, S. J. Weiss, and D. W. McCarthy, 2004: The frequency of large hail over the contiguous United States. *14th Conference on Applied Meteorology*, Seattle, WA, 3.3.

Stumpf, G. J., T. M. Smith, and J. Hocker, 2004: New hail diagnostic parameters derived by integrating multiple radars and multiple sensors. Preprints, *22nd Conf. On Severe Local Storms*, Hyannis, MA, Amer. Meteor. Soc., CD-ROM, P7.8.

Straka, J., 2009: *Cloud and Precipitation Microphysics: Principles and Parameterizations*. Cambridge Univ. Press, 1st Edition, 406 pp.

Torres, S. M, and C. D. Curtis, 2007: Initial implementation of super-resolution data on the NEXRAD network. *23rd International Conf. on Interactive Information Processing Systems,* San Antonio, TX, Amer. Meteor. Soc., CD-ROM, 5B.10.

Trapp, R. J., D. M. Wheatley, N. T. Atkins, R. W. Przybylinski, and R. Wolf, 2006: Buyer beware: Some words of caution on the use of severe wind reports in postevent assessment and research. *Wea. Forecasting*, **21**, 408-415.

Tuovinen, J. P., A. J. Punkka, J. Rauhala, H. Hohti, and D. Schultz, 2009: Climatology of severe hail in Finland: 1930-2006. *Mon. Wea. Rev.*, **137**, 2238-2249.

Waldvogel, A., B. Federer, and P. Grimm, 1979: Criteria for the detection of hail cells. *J. Appl. Meteor.*, **18**, 1521-1525.

Wilson, C. J., K. L. Ortega, and V. Lakshmanan 2009: Evaluating multi-radar, multi-sensor hail diagnosis with high resolution hail reports. Preprints, *25th Conf. on Interactive Information Processing Systems,* Phoenix, AZ, Amer. Meteor. Soc., CD-ROM P2.9.

Wilks, D. S., 2006: *Statistical Methods in the Atmospheric Sciences*. 2nd ed. Elsevier, Inc. 627 pp.

Witt, A., M. D. Eilts, G. S. Stumpf, J. T. Johnson, E. D. Mitchell, and K. W. Thomas, 1998a: An enhanced hail detection algorithm for the WSR-88D. *Wea. Forecasting*, **13**, 286-303.

Witt, A., M. D. Eilts, G. S. Stumpf, E. D. Mitchell, J. T. Johnson, and K. W. Thomas, 1998b: Evaluating the performance of WSR-88D Severe Storm Detection Algorithms. *Wea. Forecasting*, **13**, 513-518.

Wyatt, A., and A. Witt, 1997: The effect of population density on ground-truth verification of reports used to score a hail detection algorithm. *28th Conference on Radar Meteorology*, Austin, TX, Amer. Meteor. Soc., pp. 368-369.

Xie, B., Q. Zhang, and Y. Wang, 2010: Observed characteristics of hail size in four regions in China during 1980 – 2005. *J. Climate*, **23**, 4973-4982.

List of Figures

FIG. 1. From Wilson et al. (2009). Illustrates the definitions for hit (H), false alarm (FA), miss (M) and correct null (CN), which were used in calculating the HSS to find optimal MESH thresholds for “any hail” and “severe hail.”

FIG. 2. (Top) HSS as a function of MESH threshold. Point matching, as well as maximum and median MESH within a 2 km search radius about each SHAVE report were used for the scoring. (Bottom) HSS by region for any hail (21 mm), severe hail (29 mm), and the maximum HSS (the value above the maximum bar represents the MESH size where maximum was achieved for the severe hail threshold). The regions consist of four quadrants dividing the U.S. east of the Rocky Mountains (see text).

FIG. 3. Portion of a daily MESH grid from the Midwest U.S. on 18 June 2009. This is the result of accumulating MESH grids with 5-minute temporal resolution, taking the maximum value at every point. MESH swaths from individual storms can be seen clearly. Blue shades represent areas with any MESH, yellow shades represent areas with non-severe hail (21 mm ≤ MESH < 29 mm), and red shades represent areas of severe hail (MESH ≥ 29 mm).

FIG. 4. Maximum MESH for 2007-2010. Blue shades represent areas with any MESH, yellow shades represent areas with non-severe hail (21 mm ≤ MESH < 29 mm), and red shades represent areas of severe hail (MESH ≥ 29 mm).

FIG. 5. 2007-2010 annual hail days per year.

FIG. 6. 2007-2010 annual severe hail days per year.

FIG. 7. Average monthly severe hail days for a) January, b) February, c) March, d) April, e) May, and f) June.

FIG. 8. Average monthly severe hail days for a) July, b) August, c) September, d) October, e) November, and f) December.

FIG. 9. 2007-2010 annual severe hail days, using event day methodology with radar-based criteria.

FIG. 10. As in FIG. 9, but with reports-based criteria.

FIG. 11. 2007-2010 average severe hail days difference (reports-based minus radar-based).

FIG. 12. NEXRAD coverage below 10,000 ft. AGL. The level refers to the bottom of the beam height (assuming Standard Atmospheric Refraction). Terrain blockage indicated where 50% or more of the beam is blocked.

TABLE 1. 2D MRMS and velocity-derived products created for the MYRORSS database.

MergedReflectivityQC Composite	Maximum Expected Size of Hail (MESH)	60-dBZ Echo top
Height of reflectivity at lowest level	Probability of Severe Hail (POSH)	50-dBZ Echo top
Lowest level reflectivity	Severe Hail Index (SHI)	30-dBZ Echo top
Reflectivity at -20^{o}C	Vertically Integrated Liquid (VIL)	18-dBZ Echo top
Reflectivity at -10^{o}C	Height of 50-dBZ echo above 0^{o}C	0-2 km AGL Merged AzShear
Reflectivity at 0^{o}C	Height of 50-dBZ echo above -20^{o}C	3-6 km AGL Merged AzShear
Layer average reflectivity -20^{o}C to 0^{o}C	Height of 30-dBZ echo above -10^{o}C	

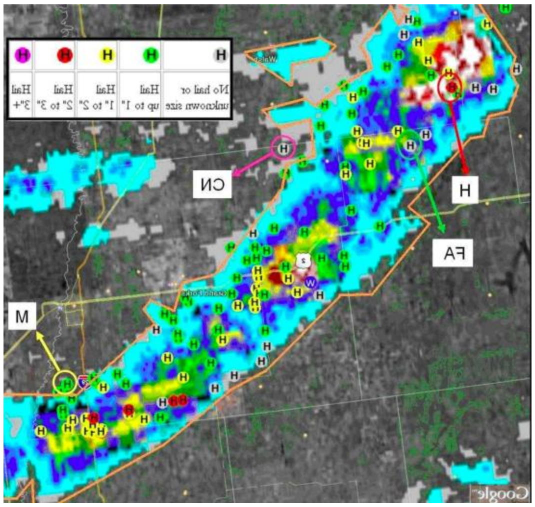

FIG. 1. From Wilson et al. (2009). Illustrates the definitions for hit (H), false alarm (FA), miss (M) and correct null (CN), which were used in calculating the HSS to find optimal MESH thresholds for “any hail” and “severe hail.”

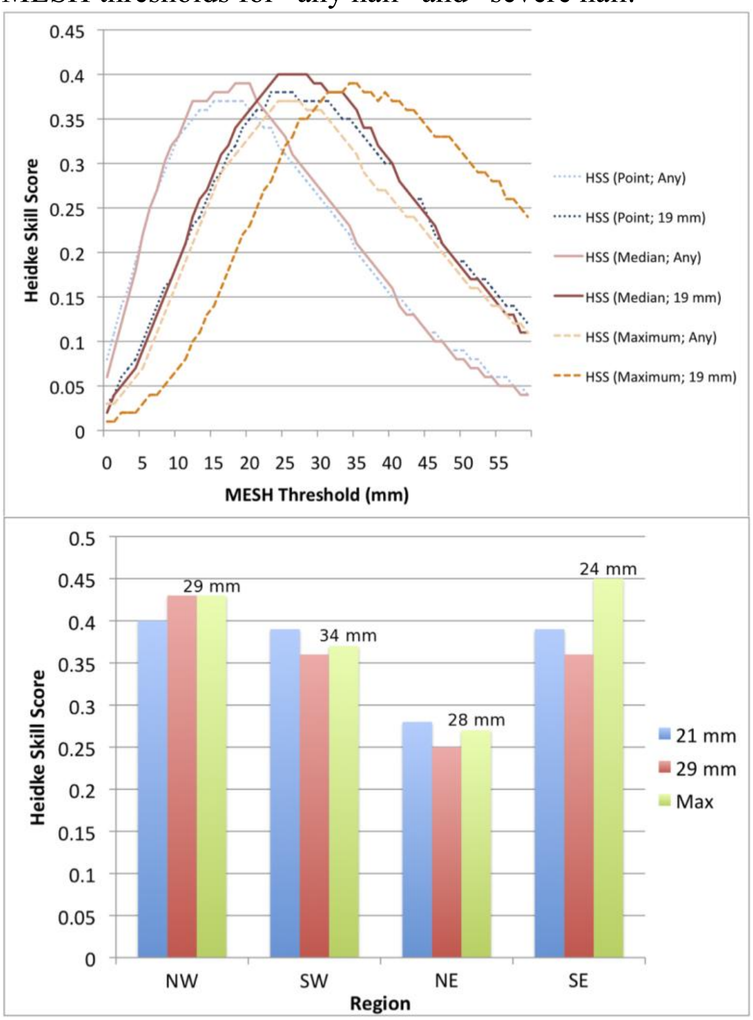

FIG. 2. (Top) HSS as a function of MESH threshold. Point matching, as well as maximum and median MESH within a 2 km search radius about each SHAVE report were used for scoring. (Bottom) HSS by region for any hail (21 mm), severe hail (29 mm), and the maximum HSS (the value above the maximum bar represents the MESH size where maximum was achieved for the severe hail threshold). The regions consist of four quadrants dividing the U.S. east of the Rocky Mountains (see text).

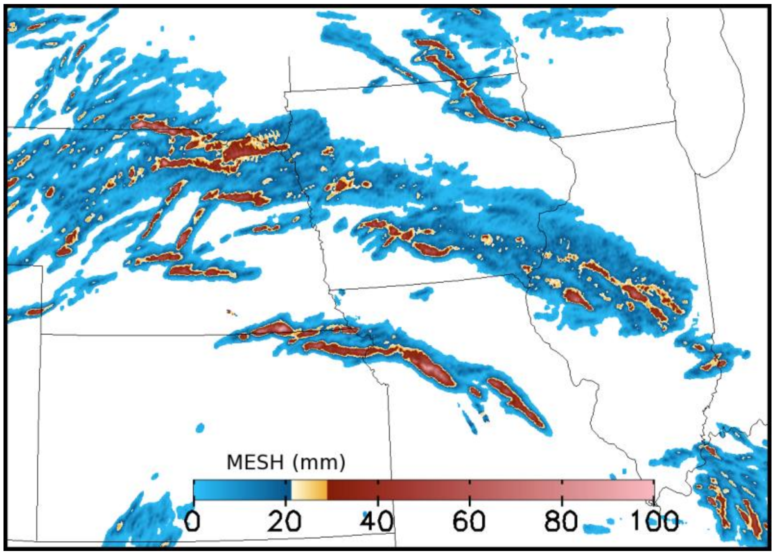

FIG. 3. Portion of a daily MESH grid from the Midwest U.S. on 18 June 2009. This is the result of accumulating MESH grids with 5-minute temporal resolution, taking the maximum value at every point. MESH swaths from individual storms can be seen clearly. Blue shades represent areas with any MESH, yellow shades represent areas with non-severe hail ($21 \text{ mm} \leq \text{MESH} < 29 \text{ mm}$), and red shades represent areas of severe hail ($\text{MESH} \geq 29 \text{ mm}$).

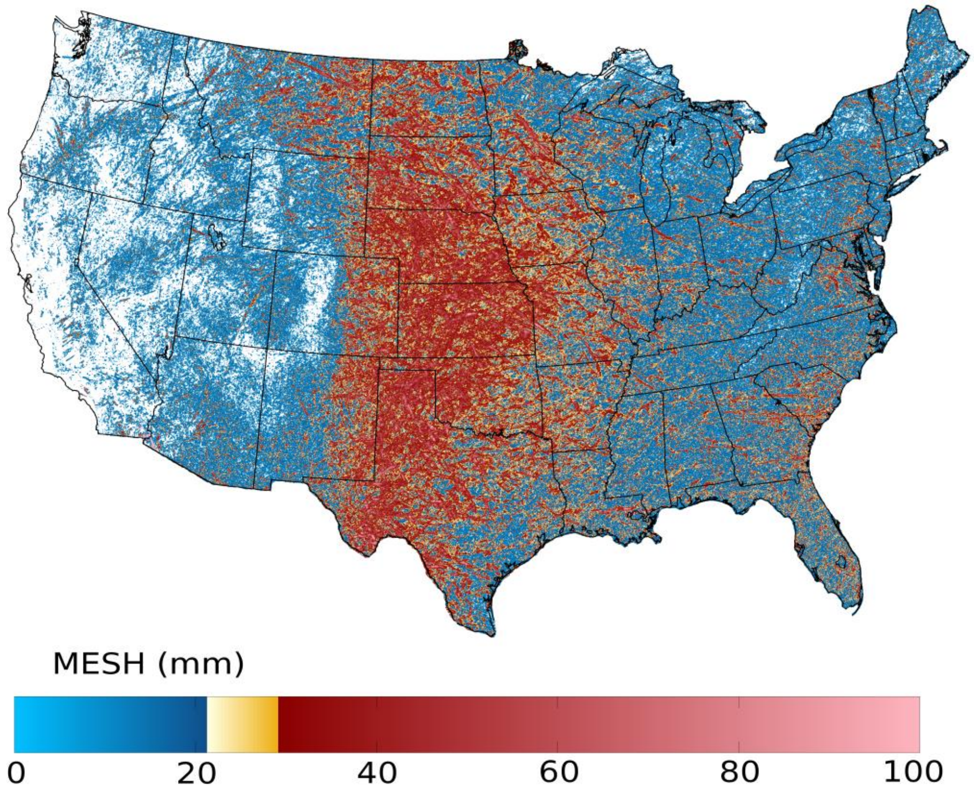

FIG. 4. Maximum MESH for 2007-2010. Blue shades represent areas with any MESH, yellow shades represent areas with non-severe hail (21 mm ≤ MESH < 29 mm), and red shades represent areas of severe hail (MESH ≥ 29 mm).

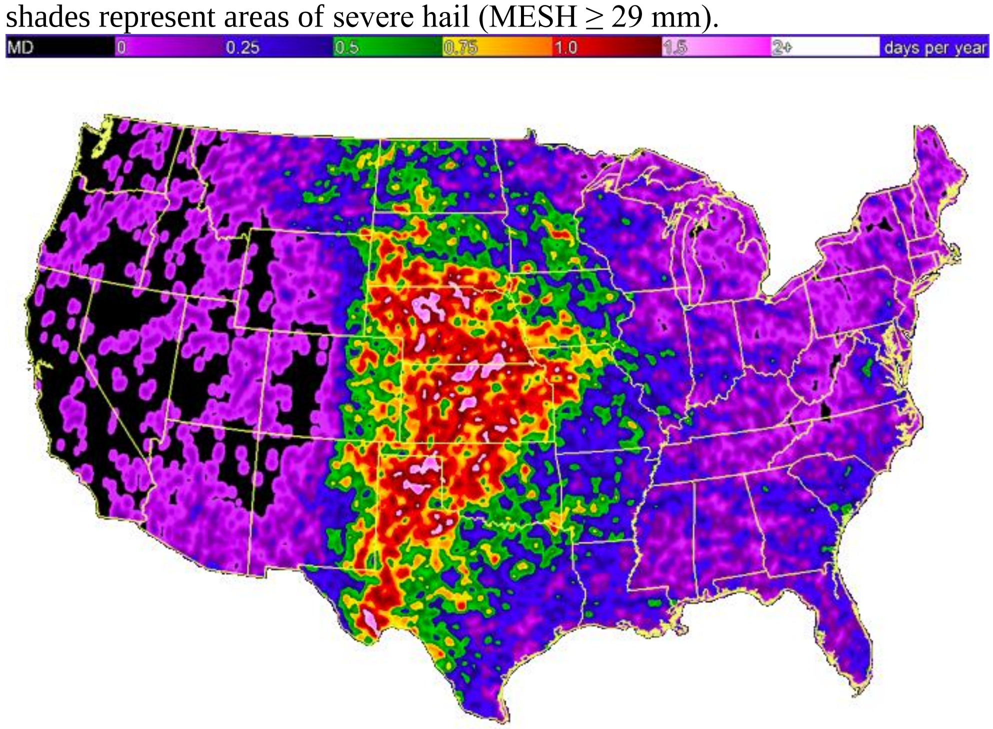

FIG. 5. 2007-2010 annual hail days per year.

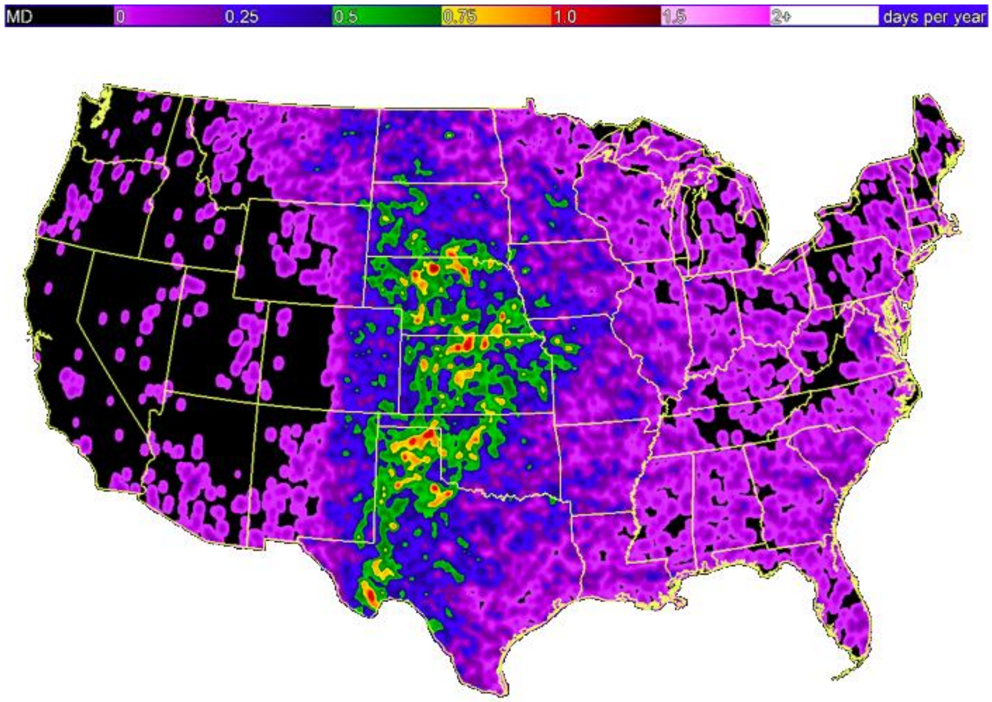

FIG. 6. 2007-2010 annual severe hail days per year.

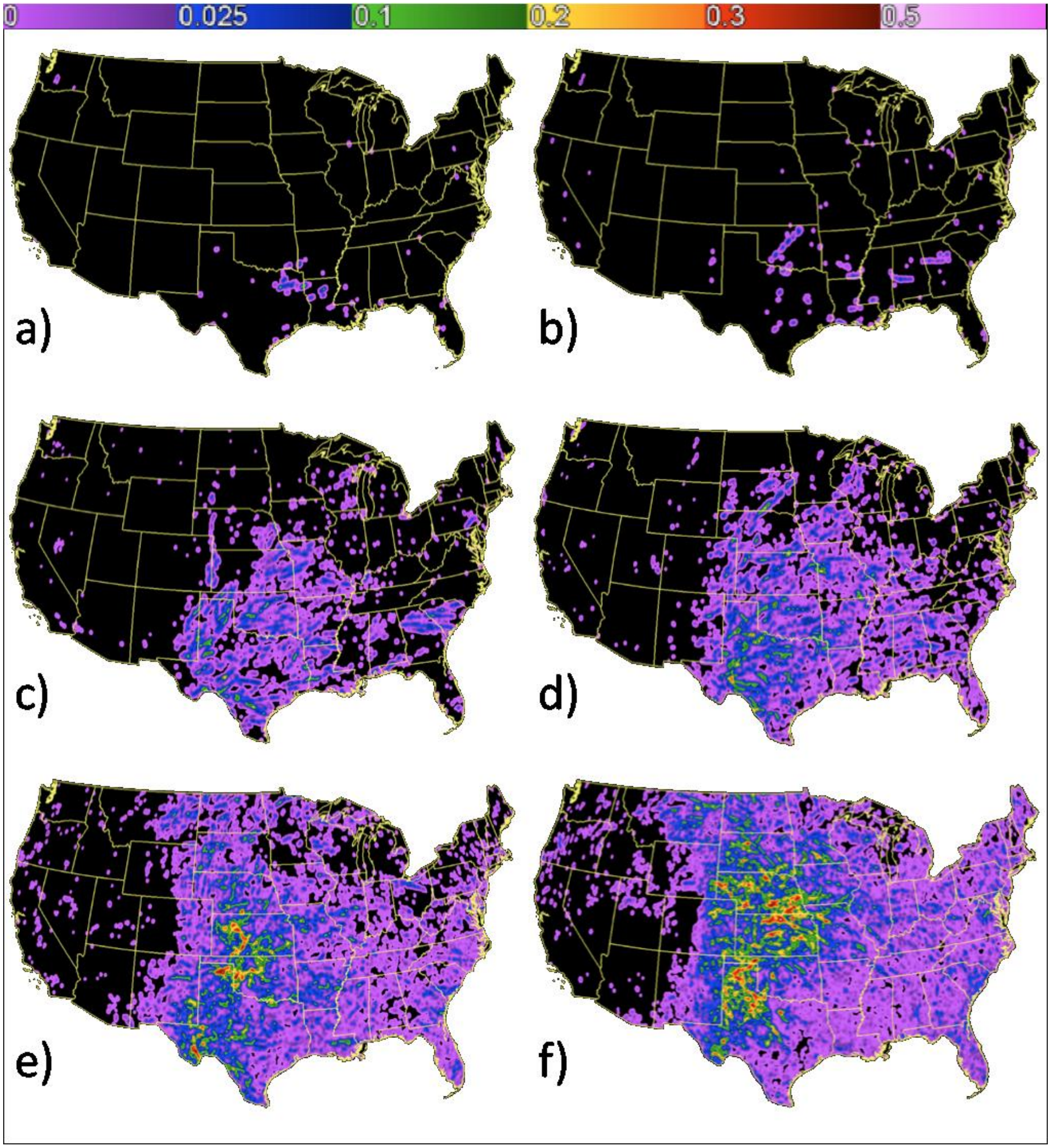

FIG. 7. Average monthly severe hail days for a) January, b) February, c) March, d) April, e) May, and f) June.

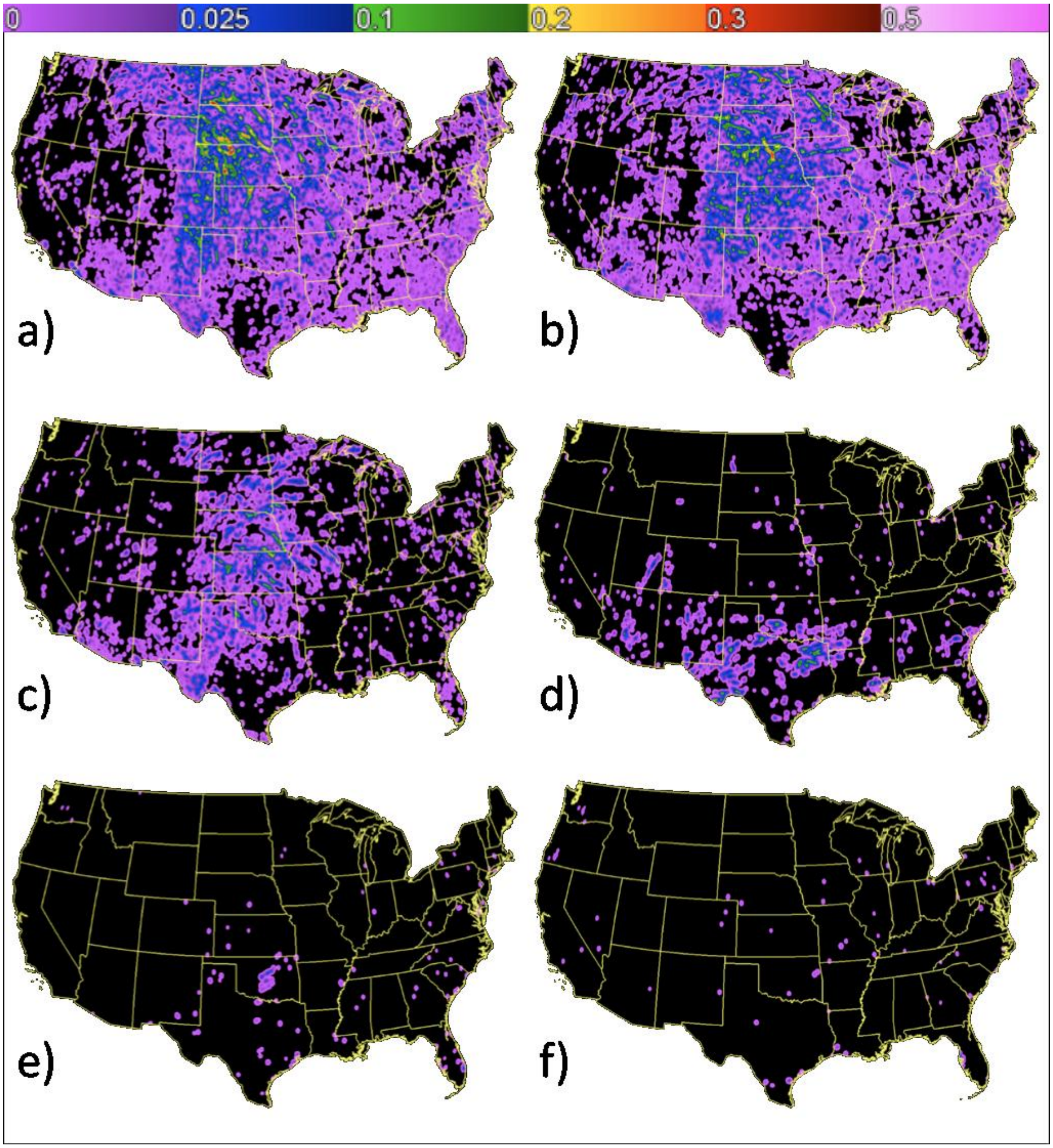

FIG. 8. Average monthly severe hail days for a) July, b) August, c) September, d) October, e) November, and f) December.

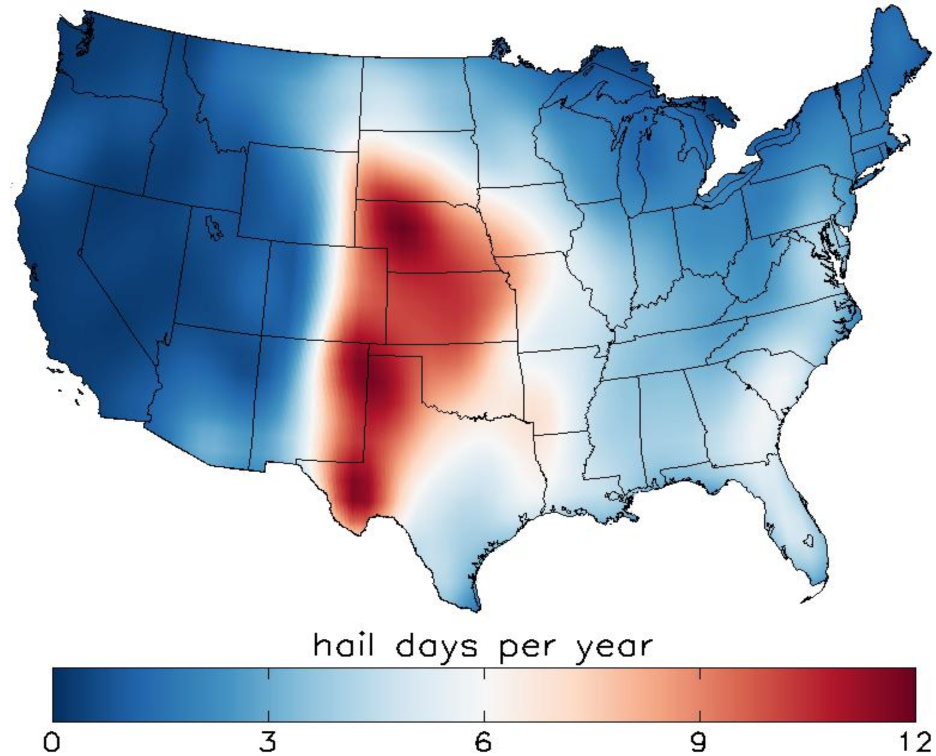

FIG. 9. 2007-2010 annual severe hail days, using event day methodology with radar-based criteria.

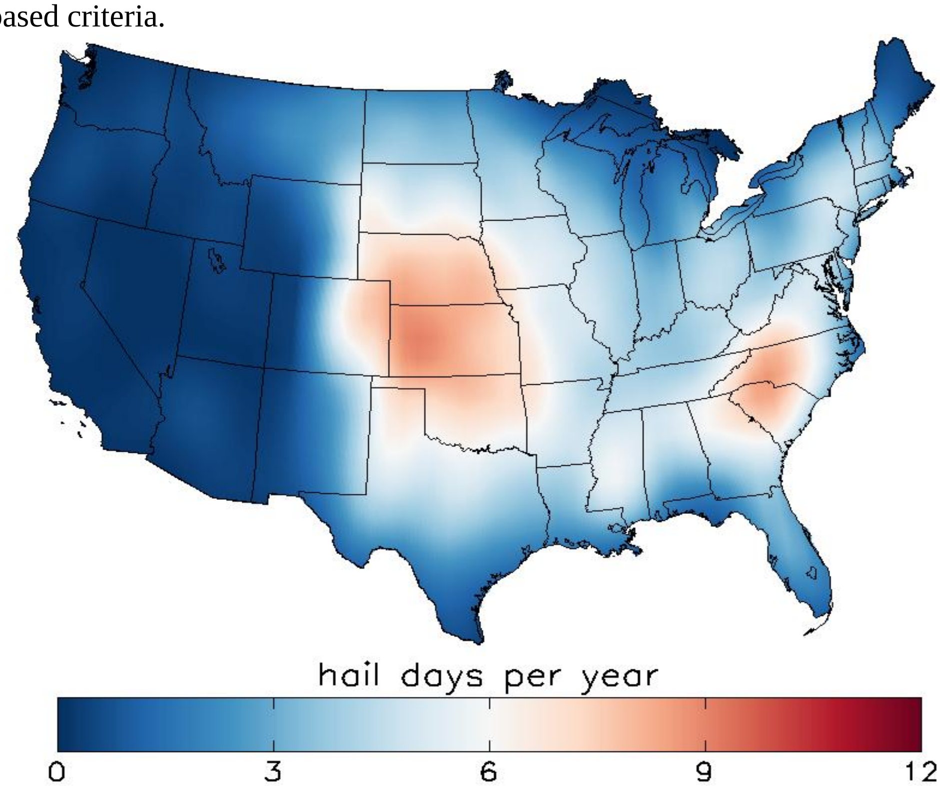

FIG. 10. As in FIG. 9, but with reports-based criteria.

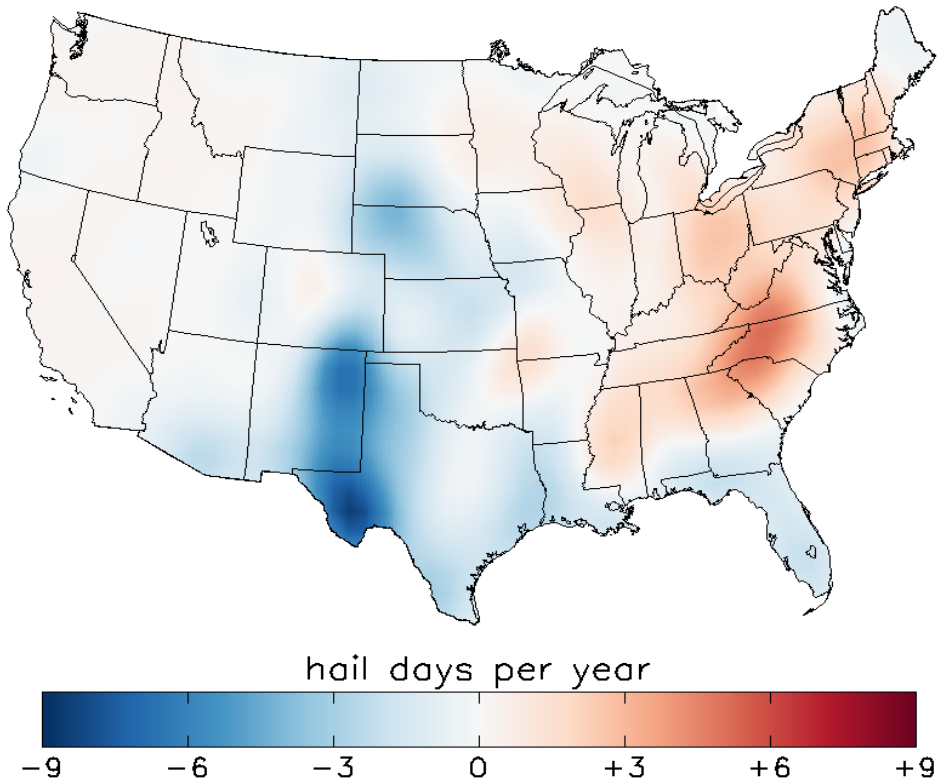

FIG. 11. 2007-2010 average severe hail days difference (reports-based minus radar-based).

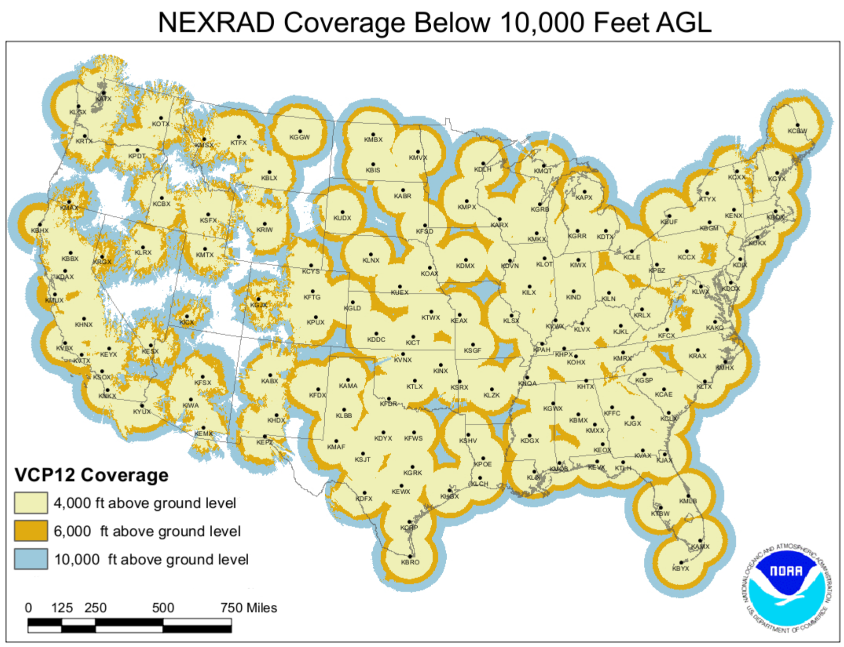

FIG. 12. NEXRAD coverage below 10,000 ft. AGL. The level refers to the bottom of the beam height (assuming Standard Atmospheric Refraction). Terrain blockage indicated where 50% or more of the beam is blocked.